Minerals Engineering 174 (2021) 107270

Contents lists available at ScienceDirect

Minerals Engineering

journal homepage: www.elsevier.com/locate/mineng

Linking molecular structures of yeast-derived biosurfactants with their foaming, interfacial, and flotation properties

Priyanka Dhar [a], Maria Thornhill [a], Sophie Roelants [c,d], Wim Soetaert [c,d], Irina V. Chernyshova [a,b,*], Hanumantha Rao Kota [a,*]

[a] Department of Geoscience and Petroleum Engineering, Norwegian University of Science and Technology, NO-7031 Trondheim, Norway
[b] Department of Environmental Engineering, Columbia University, New York, NY 10027, USA
[c] Bio Base Europe Pilot Plant, Rodenhuizekaai 1, 9042 Ghent, Belgium
[d] Centre for Industrial Biotechnology and Biocatalysis (InBio.be), Department of Biotechnology (BW25), Faculty of Bioscience Engineering, Ghent University, Coupure Links 653, 9000 Ghent, Belgium

ARTICLE INFO

Keywords:
Froth flotation
Copper sulfides
Biosurfactants
Green collectors
Foaming properties
Surface tension
Contact angle

ABSTRACT

Yeast-derived bola amphiphiles have attracted growing attention in various industrial sectors as green reagents. However, their physico-chemical properties relevant to mineral separation by froth flotation are poorly explored. To bridge this gap, we studied the foaming, interfacial, and flotation properties of acidic sophorolipid (ASL), acidic glucolipid (GL) and alcoholic glucoside (GS) obtained from strain engineering of the yeast *Candida bombicola* by molecular editing of the headgroups. Bench-scale flotation testing of a copper sulfide ore showed that ASL can effectively separate copper sulfides (85% recovery at 20% grade), GL is less effective (ca. 60% recovery and 13% grade), while GS is a poor collector. To understand this trend, we studied the interfacial and foaming properties of these three biosurfactants. The surface tension study reveals that, contrary to GS, self-assembly of both ASL and GL at the air–water interface is pH-responsive, suggesting that both the biosurfactants acquire a Π-shape. The dependence of the foaming properties of all the three surfactants on pH and concentration does not correlate with the trends in the static surface tension, suggesting the critical roles of dynamic factors, interfacial elasticity and interfacial viscosity. Hydrophobicity of djurleite (a model copper sulphide) in the presence of the three surfactants was assessed using the contact angle and Hallimond flotation methods. ASL and GL only float the pure mineral at alkaline pH, which is consistent with the contact angle data. In contrast, even though GS does not have a significant effect on contact angle, it floats djurleite in a wide pH range, which is explained by the mechanical entrainment of hydrophilic mineral particles in rich GS foams. Overall, these results demonstrate the potential of carboxylic bola biosurfactants for the recovery of copper sulfides from ores. They also bring new insights into the interfacial and foaming properties of bola biosurfactants, which can assist their introduction into other industries.

1. Introduction

The strengthening of safety, health and environmental regulations discourages the use of toxic reagents in flotation, driving their replacement by green alternatives. In this context, there is growing interest in biosurfactants (surfactants produced by microbes or yeasts from renewable resources) due to their low eco-toxicity and increased biodegradability and biocompatibility compared to conventional petroleum-based counterparts (Jain et al., 2020).

Previous investigation into the development of green substitutes for conventional petroleum-based flotation reagents has so far focused mostly on microorganisms rather than their metabolites including biosurfactants (Jain, et al., 2020; Rao et al., 2010). As a result, there is no systematic knowledge on biosurfactants as flotation reagents, though prior work demonstrates that biosurfactants can be used as collectors and frothers. In particular, it has been found that rhamnolipids, lipopeptides and non-disclosed biosurfactants can float iron oxides, silicates, and coal (Zouboulis et al., 2003; Szymanska and Sadowski, 2010;

* Corresponding authors at: Department of Geoscience and Petroleum Engineering, Norwegian University of Science and Technology, NO-7031 Trondheim, Norway (I.V. Chernyshova).
E-mail addresses: irina.chernyshova@ntnu.no (I.V. Chernyshova), hanumantha.rao.kota@ntnu.no (H. Rao Kota).

https://doi.org/10.1016/j.mineng.2021.107270
Received 7 May 2021; Received in revised form 12 October 2021; Accepted 13 October 2021
Available online 22 October 2021

Khoshdast et al., 2011; Didyk and Sadowski, 2012; Olivera et al., 2019; Pereira et al., 2021; Augustyn et al., 2021). Rhamnolipids can also be used as frothers (Fazaelipoor et al., 2010; Khoshdast et al., 2012). However, they negatively affect flotation of Cu and Mo sulfide minerals with thionocarbamate and dithiophosphatetype as collectors (Khoshdast et al., 2012). At the same time, rhamnolipids improve the recovery of pyrite and iron oxides (Khoshdast et al., 2012).

Within a very diverse class of biosurfactants, three glycolipid biosurfactants shown in Fig. 1 are of special interest due to their bipolar (bola) molecular structures and the relatively high technological level of their production. These surfactants have a C18 hydrocarbon chain with a C9 unsaturation (derived from the tail of oleic acid), with one end capped with a saccharide group and the other end with a carboxyl or hydroxyl group. Specifically, acidic sophorolipid (ASL) contains sophorose and carboxyl groups. This family of biosurfactants can be obtained in large amounts by the fermentation process of the yeast *Starmerella bombicola* and has already been commercialised for detergency and pharmaceutical applications (Roelants et al., 2016). Acidic glucolipid (GL) contains glucose and carboxyl groups. It is synthesized by *Penicillium decumbensnaringinase* and β-nitro-phenylglucoside (β-NPG) (Van Renterghem et al., 2018). Alcoholic glucoside (GS) is a by-product of the sophoroside production. It can also be produced using *Candida bombicola* cultures with glucose as the main carbon source and 2-dodecanol as the co-substrate. The interest in these bola biosurfactants as flotation collectors is stimulated by their activity in single-mineral (Hallimond) flotation of sulfide minerals (Dhar et al., 2019a; Dhar et al., 2021), which, as we elaborate below, is quite unexpected.

The efficiency of surfactants as collectors in froth flotation is defined primarily by their adsorption at the mineral–water interfaces. This reaction is driven by a decrease in the free energy of the system due to electrostatic (ion-ion and ion–dipole), chemical (covalent, ionic, and coordination bonding), hydrogen (H) bonding, hydration/dehydtarion, and chain-chain or chain-surface hydrophobic interactions (Somasundaran et al., 1998). The adsorbed surfactant renders the mineral particle hydrophobic when it exposes its hydrocarbon chain toward the aqueous solution. Packing (self-assembly) of surfactant chains at the mineral-solution interface is driven by the chain-chain and chain-mineral hydrophobic interactions (Gaudin and Fuerstenau, 1955). This process can be hampered by the incompatibility of the surfactant headgroup with the surface motif of the adsorption sites and the minimal required chain-chain distance (Ponnurangam et al., 2012). Additional complications can be imposed by the metal–surfactant precipitation and the dissolution-reprecipitation of metal ions as hydrolyzed species (autoactivation) (Dhar et al., 2021; Fuerstenau and Urbina, 1987).

Selectivity of the surfactant adsorption is underpinned mostly by the electrostatic and chemical interactions. The electrostatic interaction is controlled by pH via the surface charge of the mineral surface (established by the adsorption of H^+/OH^-) and the protonation state of the surfactant head group (controlled by its acid-base properties). Chemisorption is generally predicted by the hard and soft (Lewis) acid and bases (HSAB) concept pioneered by Pearson (Pearson, 1963) or by the stability constants of the ligand–metal complexes (Blesa et al., 2000). Within this paradigm, collectors are divided into two main groups: thio (S-donors) and non-thio (O and N donors) compounds which have different designated targets (Nagaraj et al., 2019). S-donors (e.g,. xanthates and dithiophosphates) are used as metal sulphide collectors, while O- and mixed O- and N- donors (e.g., carboxylates and hydroxamates) are used to separate metal oxides.

However, the conventional reagent-selection paradigm is challenged by the affinity of metal sulfides to polysaccharides (O-donors), especially carboxylated ones (Bicak et al., 2007; Liu et al., 2000; Moreira et al., 2017; Qiu et al., 2019; Rath et al., 2000), which is currently poorly understood (Dhar et al., 2021). It is also in conflict with the ability of acidic sophorolipid (ASL), which is an O-donor, to render djurleite ($Cu_{1.94}S$) hydrophobic at basic pH (Dhar et al., 2021). In contrast, ASL adsorption does not affect hydrophilicity of the copper sulfide at acidic pH. The single-mineral flotation follows the same trend: It step-wise increases from 40% to 75% when pH is changed from acidic to basic values. The hydrophilicity of the mineral at acidic pH has been attributed to the biosurfactant physisorption through its carboxyl group leaving the sugar group exposed to the solution. The hydrophobicity at basic pH is consistent with surface precipitation of hydrophobic Cu^{2+}-ASL complexes (Dhar et al., 2021). This non-orthodox result calls for tests of ASL on real sulfide ores, as well as a better understanding of the role of the surfactant headgroups in the surfactant performance as a sulfide collector.

Even though selective adsorption on minerals is the main performance control of a collector, its foaming properties (foamability and foam stability) are also very important. There are typically two types of foams, usually characterized by liquid content and half-life time of the foam: (i) wet and unstable, and (ii) dry and metastable. Froth flotation typically employs wet foams that are stable and fluid enough to carry the floated particles to the top of the flotation cell, while decaying quickly outside of the cell to reduce operating costs. In general, foaming properties depend on many parameters, including the film elasticity under non-equilibrium conditions, equilibrium surface Gibbs elasticity, interfacial viscosity, surface charge, steric interactions, equilibrium surface tension, disjoining pressure, and also complex surface deformation and dynamic surface tension properties (Małysa, 1992; Rosen and Kunjappu, 2012; Langevin, 2017). The main physical processes that contribute to foam destabilization are coalescence due to rupture of the films between bubbles, Ostwald ripening due to diffusion of gas (growth of large bubbles, shrinkage of small ones) and liquid drainage due to gravity (Małysa, 1992).

Since foaming properties are one of the key functional characteristics of biosurfactants in general, they have been historically among the first to study (Baccile et al., 2021). It has been found that sophorolipids in general are poor foamers (Hirata et al., 2009; Koh and Gross, 2016). Foams produced by glycolipids with sorbose and glucuronic acid headgroups are more stable than those from surfactants with a glucose headgroup (Hollenbach et al., 2020). Glycolipids with unsaturated tail groups produce foams quickly collapsing even at the smallest shear loads, whereas the branched tail group results in a higher modulus than the linear tails (Hollenbach et al., 2020). Stability of the foams produced by sophorolipid-esters with ester interrupted tail lengths ranging from 19 to 28 carbons is dominated by coalescence rather than Ostwald

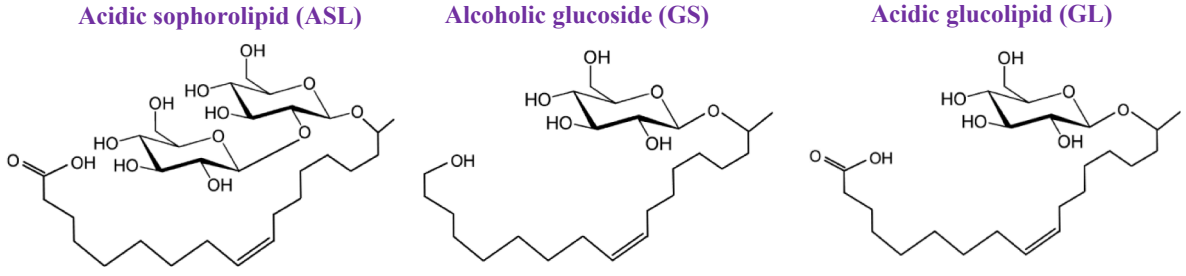

Fig. 1. Structures of bola glycolipid biosurfactants used in this study: acidic sophorolipid (ASL), glucoside (GS), and glucolipid (GL).

ripening (Koh and Gross, 2016). However, the relationship between foaming properties of the bola biosurfactants shown in Fig. 1 remains unknown. This relationship would help establish the link between the collecting and foaming properties of these biosurfactants.

The current study is a continuation of our previous work (Dhar et al., 2019a; Dhar et al., 2021), with major aims to (i) test the efficiency of the three bola biosurfactants (Fig. 1) in lab-bench flotation of a copper sulfide ore and (ii) clarify the effects of the surfactant structure on the performance of the surfactants as sulfide collectors. Toward the latter aim, we study the equilibrium surface tension and foaming properties of ASL, GL, and GS in a wide range of concentrations and pH, as well as the activity of the surfactants in hydrophobization of a model copper sulfide mineral (djurleite, $Cu_{1.94}S$) and then use these data to rationalize the lab-bench flotation results.

2. Materials and methods

2.1. Materials

ASL and GS were produced from *S. bombicola*, while GL was produced using *Penicillium decumbensnaringinase* at the Bio-base Europe pilot plant, Ghent, Belgium. The detailed procedure is described in the supplementary material (SM). Purity of the biosurfactants was 98.7% for ASL, >95% for GL, and 94.5% for GS. The characterization of impurities was performed using HPLC and GC–MS (Figs. S1 and S2). The structures of ASL (non acetylated, C18:1, molecular weigh 622), GL (non acetylated, C18:1, molecular weigh 460) and GS (non acetylated, C18:1, molecular weight 446) were confirmed using FTIR (Fig. S3). ASL is readily soluble in water. To solubilize GL and GS, solutions were heated at ca. 30° C for 10 min. Photos of the 1×10^{-5} M solutions at different pH are shown in Fig. S4.

The milli Q water (resistivity of 18.2 M Ω × cm) produced by IQ 7000, Merck, was used in surface tension and contact angle experiments. The pH was adjusted with dilute solutions of reagent grade milli Q water with HCl and NaOH. NaOH (98% pure) and HCl (98.4% pure) were from J.T. Baker. Deionized water was used in the Hallimond flotation and ore/batch flotation tests.

The djurleite ($Cu_{1.94}S$) was from Cornwall (England). Its characterization can be found elsewhere (Dhar et al., 2021). Its particles were prepared by milling in a ball mill using 660 g of stainless-steel balls (Ø1.8 mm), followed by sieving to collect the –150 + 45 μm size fraction for single mineral Hallimond tube flotation tests. Samples for contact angle experiments of the –10 μm size fractions were prepared by grinding a portion of the –45 μm material in a Fritsch P6 Pulverizette planetary mono mill at 300 rpm followed by ultrasound-assisted wet screening with a 10 μm screen.

The Nussir copper ore was provided by the Nussir ASA company of Northern Norway. The ore was characterized using ICP-MS, XRD, XRF and SEM as reported elsewhere (Dhar et al., 2019c). It has primarily chalcocite and bornite copper minerals and a small quantity of chalcopyrite at a total Cu grade of ca. 7%. A specific feature of this ore is that it practically does not contain pyrite or any other iron sulphide. Crushing and milling of this ore was performed in a jaw crusher with a 3 mm opening with subsequent sieving to the –150 μm size fraction. The dried material was sampled to provide a representative approximately 1 kg sample of each batch. 1 kg ore was ground at 60% pulp density in a stainless-steel laboratory ball mill containing the same steel balls as grinding media. A product of 80% passing size of 75-μm was achieved. The milled slurry was transferred to a 2 L batch froth flotation cell and water was added to produce a pulp density of approximately 35% solids.

2.2. Surface tension measurements

Equilibrium surface tension was measured by the Du Nouy's ring method using a computer-controlled surface tension meter (Biolin Scientific, model Sigma702). Glassware was cleaned with chromosulfuric acid. The ring was repeatedly flamed until red-hot and washed with deionized water to ensure the full removal of impurities. The instrument was first calibrated with water (72 ± 2 mN/m).

2.3. Foam preparation and characterization

The characterisation of foamability and foam stability was conducted at room temperature (25 °C) using two setups. The first one was a standard Ross-Miles foam column (Koh et al., 2017). A surfactant solution of 200 mL was placed in a pipette of specified dimensions. It had an orifice of internal diameter (i.d.) 0.0029 m and length 0.010 m. The solution in the pipette was allowed to fall from a height of 0.90 m on to 50 mL of the same solution present in a cylindrical vessel (i.d. 0.05 m) surrounded by a water jacket. The foam height in the receiver was measured immediately after the last drop of the solution fell from the foam pipette. Foam height was recorded every 30 s for 1 h.

In the second set of experiments, foams were produced and characterized with a dynamic foam analyzer DFA 100 (Krüss, Germany). The apparatus consists of a cylindrical glass column mounted in a stand with a filter paper (as an air disperser) holder at the bottom, and two vertical rows of photodiodes as light sources and light scanners. It was used for the simultaneous automatic measurement of foam (H_f) and solution (H_s) heights as a function of time. Before each experimental series, the column was carefully cleaned with a diluted Mucasol solution (Sigma-Aldrich), rinsed with a large quantity of Milli-Q water, and dried under ambient pressure. The filter paper roundel (pore size 12–15 μm) was fixed in the cylindrical glass column holder and placed in the DFA stand. Then, the column was filled with 50 mL of the prepared solution. The air was pumped through the filter paper with a flow rate of 0.5 L/min for a specific time (foaming time) equal to 20 s, and the H_f and H_s were measured by a photodiode module (blue λ = 469 nm, structure illumination 20%, height illumination 20%) and recorded by the computer using ADVANCE Software (KRÜSS GmbH). Foaming tests were performed three times, and the results were calculated as an average with standard deviation values.

2.4. Hallimond flotation

Single mineral flotation tests were performed using a 100- mL Hallimond cell (Fig. S6a). A 2 g portion of the –150 + 45 μm size fraction of the mineral was conditioned in a solution with a predetermined surfactant concentration and pH for 5 min and the suspension was transferred to the flotation cell. The flotation was conducted for 1 min at an air flow rate of 8 mL/min. The concentrate and the tailings were collected, filtered, dried, and weighed to determine the yield (recovery) of the product. Three independent experiments were performed on each sample to report their average and standard deviation.

2.5. Contact angle

Contact angle was extracted from the capillary water penetration into mineral powder beds of the –10 μm size particle fraction. The measurements were conducted using an Attension Sigma 700 apparatus (Biolin Scientific, Germany). The dried powders were packed into a tube (8 ± 0.1 mm diameter) on a filter paper over the frit on its bottom end. The tube was mounted on a probe attached to an electronic balance over a container containing water on a moving stage. Three measurements were performed on each sample to report their average and standard deviation.

2.6. Bench scale flotation

Bench scale flotation experiments were performed in a mechanical Denver bench scale flotation cell with a 2-litre volume (Fig. S6b). The mineral sample was conditioned for ten minutes with specified biosurfactant dosages. The impeller speed and air flow rate were fixed at

1200 rpm and 3 L/min. Concentrates were collected after 3, 5, 7 and 11 min after the air was introduced into the flotation cell referring to four stages of flotation. The froth was manually scraped into the collection trays with a scrape interval of 15 s. Collected samples were dried and weighed. Cu assay,%, of the feed and concentrate samples was measured using a portable Thermo Scientific Niton XL3t FPXRF spectrometer. The efficiency of the multistage Cu flotation was evaluated in terms of recoveries R and grades G (Cu assay,%, from XRF) of Cu were calculated as follows.

$$G_{\text{cumulative}} = \frac{\Sigma G_i^c \times M_i^c}{\Sigma M_i^c}$$

$$Ri = \frac{M_i^c \times G_i^c}{M^f \times G^f} 100,$$

$$R_{cumulative} = \sum R_i,$$

where G^f and G_i^c are the Cu grade of the feed and the concentrate obtained at the i^{th} stage, respectively; M^f and M_i^c are the weight of the feed and the concentrate obtained at the i^{th} stage; R_i is the recovery of the i^{th} stage. All experiments were performed in triplicate and an average result was reported.

3. Results and discussion

3.1. Equilibrium surface tension

The dependence of the equilibrium surface tension of ASL, GL and GS on concentration at pH 7.0 ± 0.6 shows that the critical micelle concentration (CMC) increases in the order ASL < GL < GS (Fig. 2a and Table 1). The CMC values of anionic ASL and GL (4×10^{-5} M and 3×10^{-4} M, respectively) are in the range typical of non-ionic surfactants, while the CMC of non-ionic GS (5×10^{-3} M) is in the CMC range of anionic surfactants (Rosen and Kunjappu, 2012; Schramm and Marangoni, 1994). This deviation from the common trend along with the significant difference between the CMC of these three surfactants indicates that, in contrast to conventional (one tail-one headgroup) surfactants, the bola biosurfactants acquire non-linear conformations at the air–water interface with the result that both their headgroups are interfacially active.

From the surface tension curves shown in Fig. 2a, we infer minimum specific surface areas, A_{min}, at pH 7 as described in the supplementary part of Dhar et al., 2021. In brief, A_{min} was calculated from the surface excess (Γ_{max}) using the following equations (Fainerman et al., 2001; Pugh and Stenius, 1985):

$$\Gamma_{\max} = -\frac{1}{\text{nRT}} \times \frac{\text{d}\gamma}{\text{dlnC}},$$

$$A_{min} = \frac{1}{N\Gamma_{max}},$$

where R is the gas constant (8.314 $J \cdot K^{-1} \cdot mol^{-1}$), N is the Avogadro's number, and n is the molecule specific dissociation number (the Gibbs prefactor). This number was taken as 1 at pH 4 and 7 on the basis of the earlier finding that ASL is weakly ionized at natural pH (Penfold et al., 2012). As seen from Table 1, all the three biosurfactants occupy high A_{min}, which is consistent with the surfactants adopting the Π-shape at the air–water interface (Scheme 1). The highest area A_{min} observed for GS can be explained by weaker intra- and inter-molecular non-covalent (electrostatic) interactions between its non-ionic headgroups as compared to ASL and GL which have a carboxylate headgroup.

Table 1
Characteristics of ASL, GL and GS at the air–water interface at pH 7.

Properties	ASL*	GL	GS
ST_{CMC} (mN/m)	38.5	40	36.3
A_{min}(Å^2)	75	73	85
CMC (mol/L)	4×10^{-5}	3×10^{-4}	5×10^{-3}

* The data for ASL were reported and discussed in detail in (Dhar et al., 2021).

The surface tension values of ASL, GL and GS with respect to pH are shown in Fig. 2b. ASL demonstrates a distinct fatty-acid-like pH dependence of the surface tension, specifically, a pronounced minimum at pH 8. As discussed elsewhere (Dhar et al., 2021), this minimum suggests that ASL adopts at the air–water interfaces a Π-shape where both the COOH/COO$^-$ and sophorose headgroups contact water, while the COOH/COO$^-$ groups of two neighbouring molecules directly interact

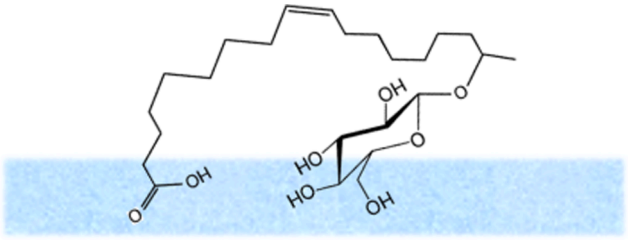

Scheme 1. Postulated Π shape of GL at the air–water-interface at neutral pH.

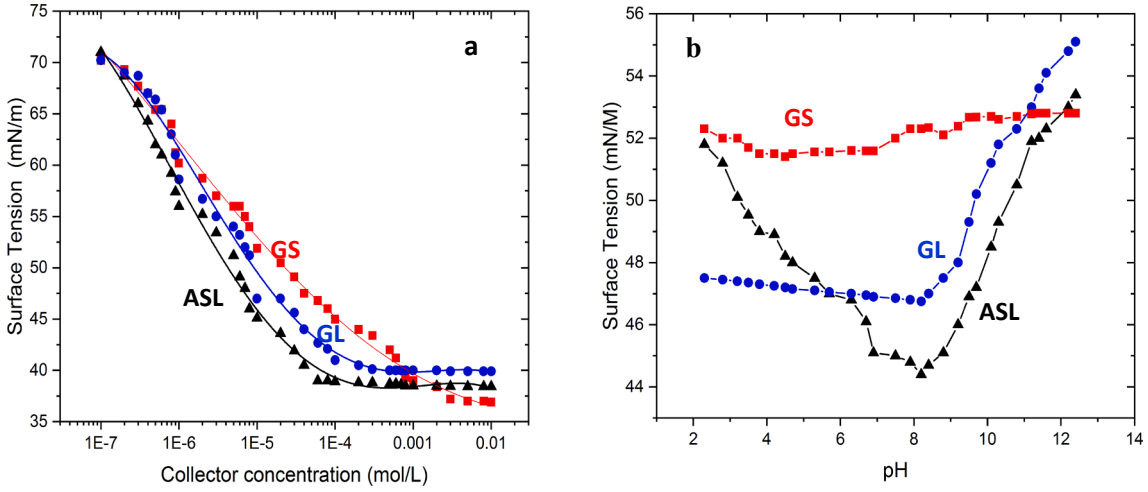

Fig. 2. Surface tension of acidic sophorolipid (ASL), acidic glycolipid (GL), alcoholic glucoside (GS) as a function of (a) surfactant concentration at pH 7 and (b) pH at a concentration of 1×10^{-5} M. The surface tension curves for ASL were reported and discussed in detail in (Dhar et al., 2021).

with one another as in the monolayer of a fatty acid. The absence of the minimum for GS (which lacks the carboxyl headgroup) supports this interpretation. GL demonstrates an intermediate case, with a much less pronounced minimum than ASL. This difference suggests that GL is less prone to organize in the $COOH/COO^-$ coupled dimers than ASL, especially at acidic pH, which can tentatively be explained by stronger interaction between the carboxylate and saccharide groups of GL. Hence, even though the high A_{min} values of GS and GL suggest that similar to ASL they adapt the Π-shape at the air–water interface, the mutual organization of the Π-shapes of these two surfactants is different. Further details could be provided by using spectroscopic, Langmuir trough, and molecular dynamics modelling methods.

3.2. Foaming properties

Foaming occurs when the surface tension of water is reduced and the system is aerated, which stabilizes a thin liquid film surrounding an immiscible gas phase (Langevin, 2017). The addition of surfactants is an effective method to reduce the interfacial tension and thereby enhance the stability of the foam film. The molecular structure and concentration of the surfactant are among the primary controls of the foaming properties, along with salinity, temperature, type of the gas, and the foam generation method (Rosen and Kunjappu, 2012).

Fig. 3 shows foamability and foam stability for ASL, GL and GS measured using the Ross-Miles setup at the surfactant concentrations of 3×10^{-5}, 3×10^{-3} and 1 M and pH 7. Increasing the surfactant concentration increases the initial foam height irrespective of the surfactant. Among the surfactants, GS has the strongest foamability and foam stability. GL has the lowest foamability, while ASL at 3×10^{-3} M and 1 M provides the lowest foam stability. In the case of ASL, the foam height drops significantly at 10 min, slowly decreasing afterward, indicating that ASL is not good as a foam stabilizer.

The same relationship between the foaming properties is observed at pH 4, 7 and 10.2 and a surfactant concentration of 3×10^{-3} M (Fig. 4). As expected, there is no effect of pH on the maximum foam height of 0.6 ± 0.2 cm attained by GS at 30 s.

GL develops the least initial foam height at pH 4, increases at pH 7, followed by an insignificant decrease at pH 10.2. ASL shows an increase in the maximum heights with increasing pH, which can be attributed to the dissociation of the carboxylic group. In the case of GS, variations in the maximum height with pH are within the experimental error. These results are in agreement with the results of the Ross-Miles test. Hence, the foaming properties of the surfactants are not directly related to their surface activity (Table 1), which can be explained by the non-equilibrium character of foams and the importance of the other effects.

To explain our findings, we should recall that foam destabilization is driven by three main physical processes: drainage of liquid out of the foam, coalescence and/or rupture of bubbles, and disproportionation (which may be called Ostwald ripening) (Langevin, 2017). Bubble coalescence could be defined as rupture of the thin liquid film between gas bubbles, forming a larger bubble whereas Ostwald ripening results mainly from the diffusion of gas from smaller to larger bubbles. It has been reported that the time scale for coalescence is generally within 10 min, whereas the time scale for Ostwald ripening is relatively long (Koh et al., 2017). While bubble coalescence and Ostwald ripening are both likely to occur in foams stabilized by the biosurfactants, the rapid decrease in foam height for ASL suggests that the dominant destabilization mechanism of the ASL foam is coalescence. In contrast, destabilization of the GS foam is likely to be Ostwald ripening. For GL, both coalescence and Ostwald ripening are anticipated to be responsible for foam destabilization. However, further studies are needed to verify these preliminary conclusions.

Previous studies have related poor stability of ASL foams to their low surface shear viscosity and/or low surface elasticity (Koh and Gross, 2016), which are likely to root from the strong lateral attraction between its headgroups at the air–water interface including strong coupling of the COO^- and COOH-capped tails (Dhar et al., 2021). Accordingly, the best foaming properties of GS can be explained by the absence of strong coupling between the surfactant headgroups at the air–water interface which increases surface elasticity. Since increasing pH increases the concentration of deprotonated carboxylate headgroups in the adsorbed surfactant monolayer, it is logical to tentatively relate the improvement of the foaming properties of ASL and GL with pH to an increase in the disjoining pressure due to electrostatic repulsion between the electric double layers of the negatively charged bubble walls.

Given the dependence of the foaming properties on the foam generation method, we performed another set of foaming measurements in the DFA apparatus. Foams were generated during 20 s and subsequently the foam decay was recorded. Fig. 5 shows the foaming properties of ASL, GL and GS at a concentration of $1x10^{-4}$ M and pH 4, 7, and 10. At 1×10^{-4} M and pH 7, the maximum height attained by both ASL and GS is approximately 80–82 mm (Fig. 5b). In contrast, GL shows an abrupt increase in the foam height as soon as the air supply starts, a plateau at 48 mm, and an abrupt drop when the air supply stops. When the foaming time is increased to 60 s (Fig. 6a), GS, ASL, and GL attain the maximum foam height at 60, 40, and 10 s, respectively. The fastest foam formation by GL implies that its diffusion or adsorption at the bubble surface is quickest, which needs to be verified using dynamic surface tension.

The maximum foam height, as observed in the DFA foam analyser, is presented as a function of the surfactant concentration at pH 7 in Fig. 6b. For all the three surfactants, a steady increase is observed at low and high concentrations, with a step-like increase at ca. 4×10^{-5} M. This step is largest for ASL and the smallest for GL. Even though this step is close to CMC of ASL, it is far below CMC of GL and GS (Table 1). This trend does not correlate with the trend observed for surface tension in Fig. 2.

The foam stability was additionally assessed using a methodology developed by (Lunkenheimer et al., 2010). This method measures changes in the foam height H_f and the solution height H_s, $\Delta H_f(t)$ and

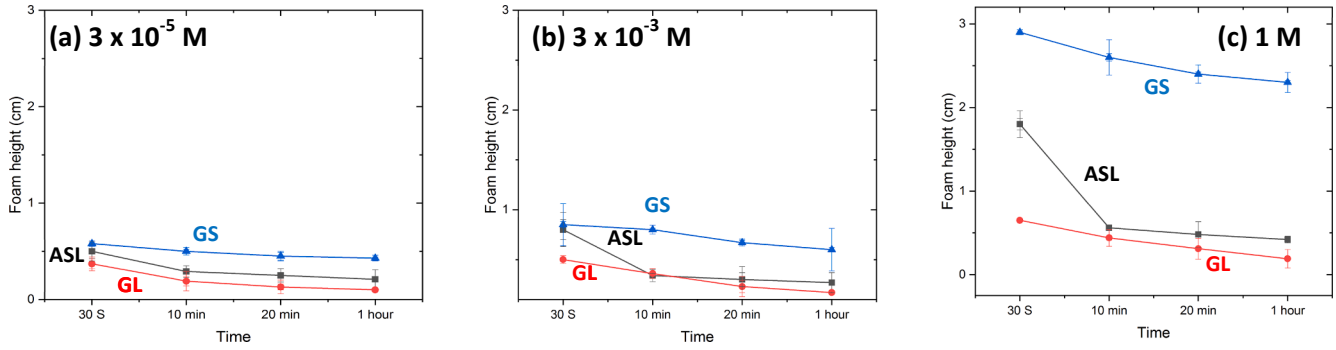

Fig. 3. Foam heights for ASL, GL, and GS at a concentration of (a) 3×10^{-5} M (b) 3×10^{-3} M and (c) 1 M. The foam heights are an average of at least three measurements at pH 7. The foam heights were obtained at constant volumetric flow of 9 L/hr introduced at the bottom of a standard Ross-Miles foam column.

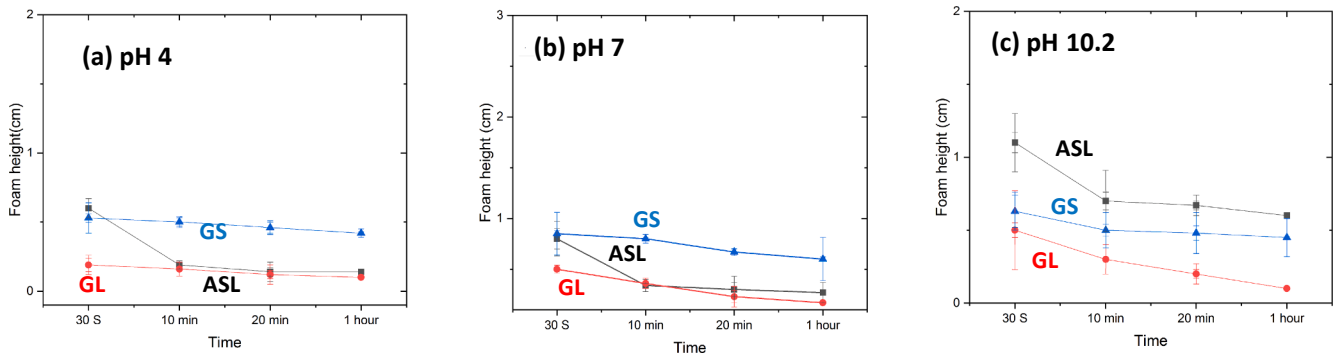

Fig. 4. Foam heights for ASL, GL, and GS at: (a) pH 4 (b) pH 7 and (c) pH 10.2 (±0.2) at a surfactant concentration of 3×10^{-3}M. Foam heights are an average of at least three measurements.

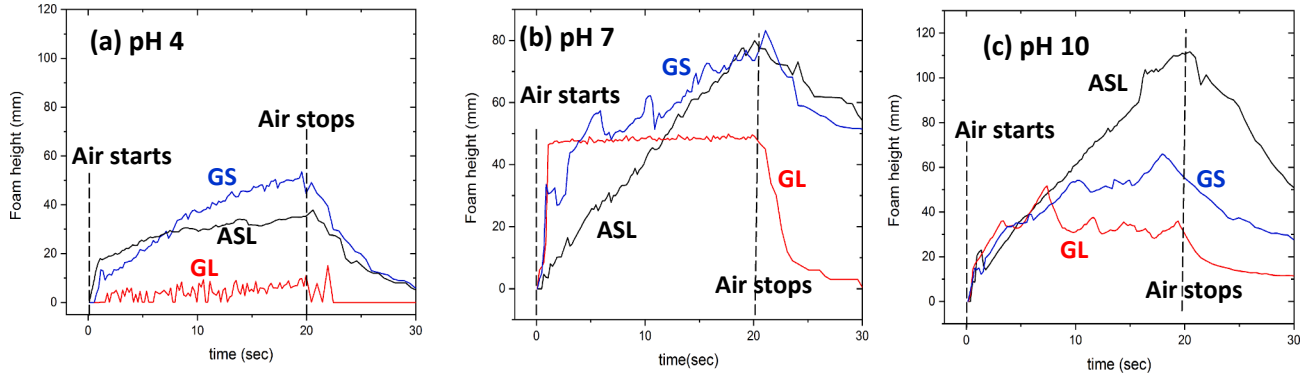

Fig. 5. Height profiles of foam formed by 1×10^{-4} M ASL, GL and GS at (a) pH 4, (b) pH 7, and (c) pH 10.2. Measurements were conducted in the DFA apparatus.

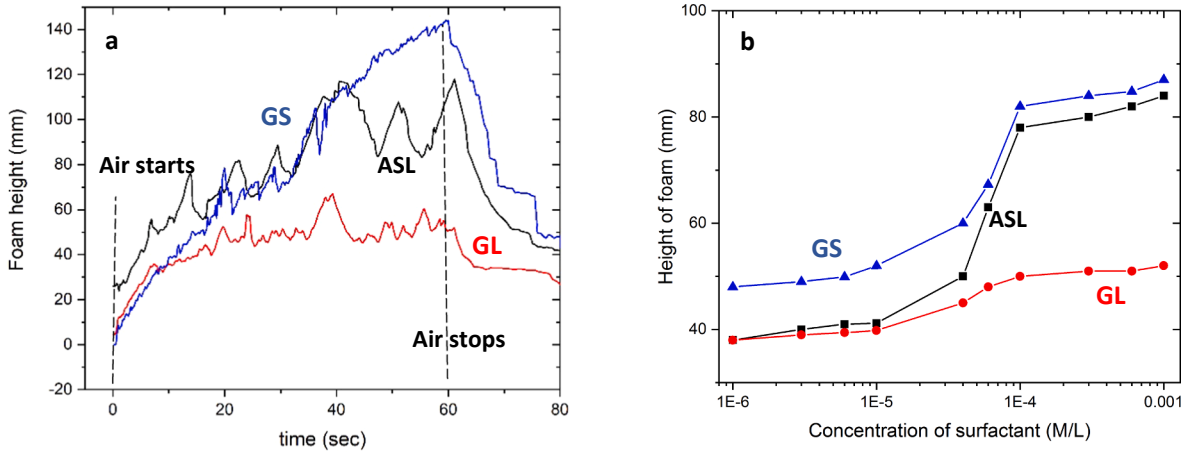

Fig. 6. Foaming properties of ASL, GL and GS at pH 7: (a) Foam height at surfactant concentration of 1×10^{-4} M as a function of time. (b) Maximum foam height (foamability) as a function of the surfactant concentration. Measurements were conducted in the DFA apparatus. Each data point in (b) is average of three readings.

$\Delta H_s(t)$, respectively:

$$\Delta H_f(t) = H_f(t_o) - H_f(t),$$

$$\Delta H_s(t) = H_s(t_o) - H_s(t),$$

where t_0 denotes the moment when the air supply was ended. A graphical presentation of the $\Delta H_f - \Delta H_s$ value as a function of time allows determining the time of deviation, t_{dev}. The latter is the time at which $\Delta H_f - \Delta H_s$ starts to be greater than 0 (Fig. 7). The value of t_{dev} is an indicator of foam stability (Lunkenheimer et al., 2010). It is the initial time interval of the foam decay, when there is only drainage of solution from the foam column but not yet any foam rupture. For t greater than t_{dev}, the process of the foam film rupture begins, and the foam column starts to decay.

The dependence of ΔH_f–ΔH_s on time t at biosurfactant concentrations of $4x10^{-5}$ M and $1x10^{-4}$ M (Fig. 7) does not reveal a significant difference between t_{dev} values for ASL and GL at these two concentrations. A noticeable difference can be observed only for GS at 1×10^{-4} M. Its t_{dev} increases from ca. 20 s at 4×10^{-5} M to 36 s at 1×10^{-4} M, indicating improvement in stability. GS, which is a strong foamer, is characterized at 4×10^{-5} M by t_{dev} as high as 20 s. This value is similar to that of dry foams of moderately stable commercial surfactants (Lunkenheimer et al., 2010). In contrast, GL is characterized by t_{dev} of 8 s,

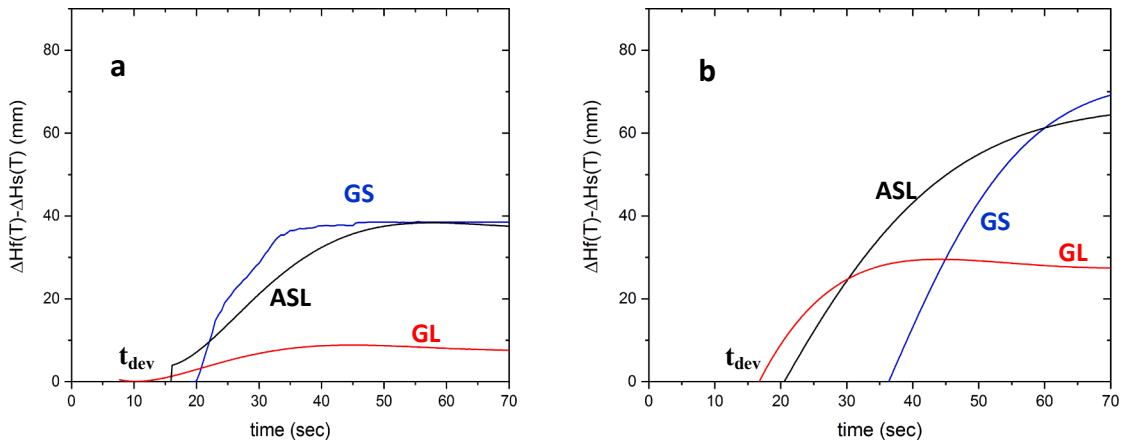

Fig. 7. Comparison of the $\Delta H_f - \Delta H_s$ parameters of ASL, GL, and GS obtained from foam heights at a surfactant concentration of (a) 4×10^{-5} and (b) 1×10^{-4} M and pH 7.

which corresponds to a wet unstable foam. ASL is characterized by an intermediate t_{dev} value of 14 sec.

Wet foams consist of spherical bubbles separated by thick liquid films (lamellae) with the liquid content usually greater than 1% (Langevin, 2017). In contrast, the liquid content in in dry foams is around <1%, while the shape of bubbles is polyhedral. Their lamella thickness is in the order of nanometers, i.e., within the range of the intermolecular forces action. Analysis of the bubble shapes in foams at 18 sec after aeration was stopped (Fig. S5) shows that foams of GL and ASL consist of spherical bubbles, whereas a polyhedral foam structure with thinner lamellae is produced by GS. Hence, non-ionic GS forms dry and moderately stable foams, whereas anionic ASL and GL form unstable wet foams which are desirable for froth flotation.

3.3. Contact angle

The contact angle was measured by employing the Washburn capillary rise method which was used to characterize hydrophobicity of the copper sulfide particles. The major problem associated with the application of this method to powders is that the contact angle depends significantly on both particle size and packing (Galet et al., 2010). Hence, we verified reproducibility of the results by three independent measurements.

As seen from Fig. 8a, the contact angle of djurleite particles conditioned in water is approximately constant (ca. 58°) at acidic pH until pH 7 and decreases by 5° with a further increase in pH due to hydroxylation of the surface. In the presence of 1×10^{-5} M ASL and GL, the contact angle increases step-wise from 38° to 70–75° at circumneutral pH and, within the experimental error of the method, remains almost the same at basic pH. This pH dependence is qualitatively different from that observed for other anionic collectors below CMC. Their hydrophobicity always goes down at highly alkaline pH (though there can be a second maximum) due to the electrostatic repulsion of anionic surfactants from the negatively charged mineral surface (Theander and Pugh, 2001). Our previous study has demonstrated that the hydrophobicity of djurleite at alkaline pH in the presence of ASL can be explained by the ASL adsorption in the form of hydrophobic Cu(II)-ASL precipitates, while hydrophilicity at acidic pH is consistent with the ASL adsorption through the carboxylic group (Dhar et al., 2021). This model can be applied to GL, given its structural similarity to ASL. In contrast, djurleite conditioned with GS is characterized in the wide pH range by similar contact angles as in water, which indicates a negligible influence of GS on hydrophobicity. To interpret this result, we take into account that the contact angle of the gold surface increases from 48° to 55° when oleate is grafted to the surface through the carboxylate group (Valotteau et al., 2015). In contrast, the contact angle remains unchanged when the surface is functionalized by ASL grafted through its carboxylate group and exposing its sophorose group towards the solution (Valotteau et al., 2015). On this basis, we conclude that either GS is negligibly adsorbed on the mineral surface or adsorbed through only one its headgroups.

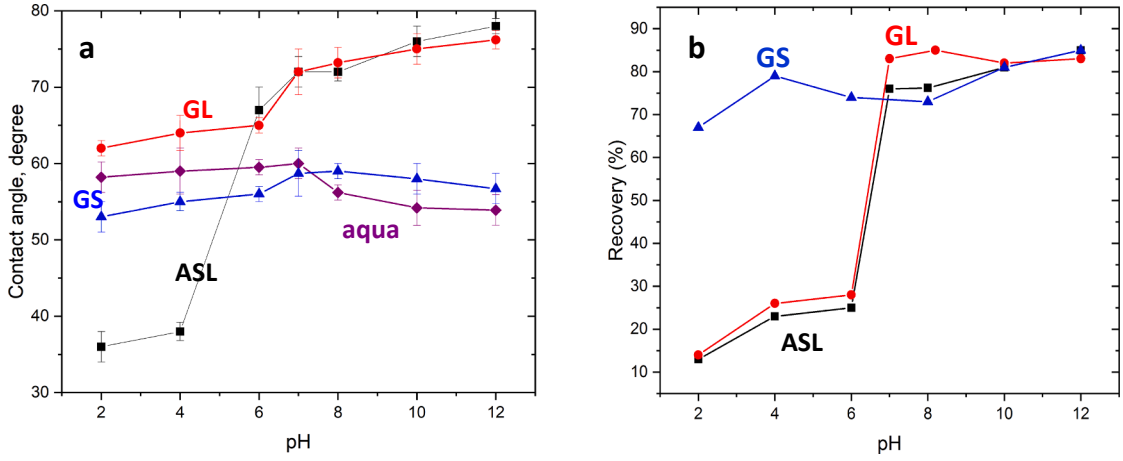

Fig. 8. (a) Contact angle of djurleite as a function of pH in the presence of ASL, GL, and GS at a concentration of 1×10^{-5}M and pH 7. (b) Hallimond flotation of djurleite (1 min) in the presence of $1x10^{-5}$ M ASL, GL and GS as a function of pH. The contact angle curves for ASL were reported and discussed in detail in (Dhar et al., 2021).

3.4. Hallimond flotation

As seen from Fig. 8b, the pH dependence of the floatability of djurleite particles in a Hallimond cell in the presence of 1×10^{-5}M ASL and GL is consistent with the pH dependence of the contact angle (Fig. 8a). Specifically, a recovery of 75–85% is observed at pH higher than 6, while the recovery is below 30% at acidic pH, which supports for GL the adsorption model previously proposed for ASL (Dhar et al., 2021). In contrast, an apparent inconsistency is observed for GS. This biosurfactant achieves a high recovery of 75–85% in the whole pH range, while the corresponding contact angle is similar to that observed in the absence of the surfactant. This result reinforces the notion that the single mineral flotation does not necessarily follow the contact angle trend. Given the superior foaming properties of GS (Figs. 3–7) and its weak effect on the contact angle (Fig. 8a), its capacity to recover the mineral in the broad pH range can be attributed to mechanical entrainment.

3.5. Bench scale flotation

Bench-scale flotation tests in the presence of ASL, GL and GS were performed at natural pH of ca.9.2 on a copper ore obtained from the Nussir deposit. A specific feature of this ore is that it does not contain pyrite or any other iron sulphide. Therefore, concentration of copper from this ore would be feasible at natural pH.

Sufficient froth stability is a mandate in bench-scale flotation tests for the concentrate to transfer into a froth phase, while still allowing for the drainage of hydrophilic particles out of the froth. We found that the levels of entrainment for all the three biosurfactants are high, while the drainage is insufficient resulting in low concentrate grades. Therefore, we measured the cumulative water recovery, which is a strong indicator of entrainment due to froth stability (Warren, 1985; Ross, 1989) to correlate with the cumulative solid recovery.

As seen from Fig. 9a, the cumulative solid recovery with ASL and GL is constant after 5 min, indicating that the flotation results are not merely due to mechanical entrainment, and these two surfactants act as collectors. The recovery of copper in flotation with ASL and GL is high, close to 85% and 68% respectively (Fig. 9b). Additionally, the grades are approximately 12 and 20% in the presence of GL and ASL respectively. In the presence of ASL, over a longer period of time, cumulative recovery of copper increased from 40 to 85% but the grade decreased from 25 to 18%. Similarly, in the presence of GL, although the recovery increased from 40 to 65%, grades decrease from 20 to 12%. The grade-recovery curve shows that in both cases, most of the copper minerals are floated by the end of 5 min, followed by a steep fall beyond this flotation time. Both the grade and recovery are significantly lower with GS compared to ASL and GL. This result confirms the above conclusion based on the contact angle and Hallimond flotation data that GS floats copper minerals through the physical pathway due to its high frothing capacity. In our recent work on the same ore using three commercial thiol reagents (xanthate, dithiophosphates and thionocarbamates) we observed that the best cumulative recovery and grade at 89% and 22% were achieved by thionocarbamate (DTC) (Dhar et al., 2019b) (Fig. 9b). These results are comparable to ASL, thus indicating that, despite being an O-donor, ASL holds promise as a green collector in copper sulfide flotation.

4. Conclusions

As part of the effort towards the introduction of biosurfactants to mineral separation by froth flotation, this study links the performance of three bola biosurfactants, ASL, GL, and GS (Fig. 1) in the selective recovery of copper sulfides from a sulfide ore with their interfacial and foaming properties. We found that

(1) The equilibrium surface tension values of ASL and GL strongly depend on pH, whereas no significant effect is observed for GS.
(2) The dependence of surface tension on pH suggests that GL, similarly to ASL, acquires at basic pH at the air–water interface a Π-shape where the COOH/COO^- headgroups of two neighbors are coupled by non-covalent interactions.
(3) Among the three biosurfactants, GS demonstrates the best foaming properties.
(4) As-created GS foams are dry and stable, whereas foams produced by ASL and GL at neutral pH are wet and unstable.
(5) ASL and GL increase hydrophobicity of djurleite step-wise at basic pH, as follows from the contact angle and Hallimond flotation results.
(6) GS does not have a significant effect on the contact angle of djurleite, even though it promotes Hallimond flotation of the pure mineral.
(7) Bench-scale flotation of a copper ore demonstrates that ASL can compete with conventional thiol collectors in flotation of copper sulfides. GL is less efficient than ASL. In contrast, GS is not efficient as a sulfide collector, which is explained by non-selective transport of the ore particles by the rich foam.

The reported foaming properties of the yeast-derived bola biosurfactants can be of interest for their application as frothing agents in

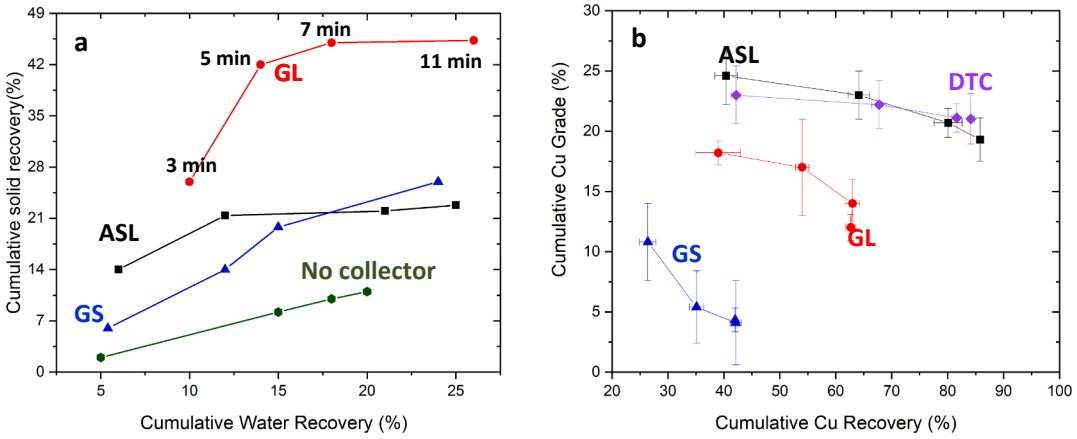

Fig. 9. (a) Cumulative water–solid recovery and (b) Cumulative copper recovery and grade demonstrated by ASL (squares), GL (red circles) and GS (triangles) at pH 9.2 at a surfactant concentration of 1×10^{-5} M. Concentrates were collected at 3, 5, 7 and 11 min. For comparison purposes, graph (b) includes flotation results obtained on the same ore with 1×10^{-5} M thionocarbamate (DTC) (diamonds) at pH 8.2 (Dhar et al., 2019b). (For interpretation of the references to colour in this figure legend, the reader is referred to the web version of this article.)

various industrial applications, while the high selectivity and recovery of copper from a copper ore with ASL suggests their potential in the froth flotation of sulphides.

CRediT authorship contribution statement

Priyanka Dhar: Methodology, Investigation, Formal analysis, Writing – original draft. **Maria Thornhill:** Supervision, Writing – review & editing. **Sophie Roelants:** Resources. **Wim Soetaert:** Resources. **Irina V. Chernyshova:** Conceptualization, Supervision, Methodology, Validation, Writing – original draft, Writing – review & editing, Resources. **Hanumantha Rao Kota:** Conceptualization, Supervision, Methodology, Resources.

Declaration of Competing Interest

The authors declare that they have no known competing financial interests or personal relationships that could have appeared to influence the work reported in this paper.

Acknowledgments

IVC and HRK gratefully acknowledge the financial support of the Research Council of Norway (NFR), FRINATEK Project No.: 274691. PD and IVC thank financial support of the Department of Geoscience and Petroleum, NTNU.

Appendix A. Supplementary material

Supplementary data to this article can be found online at https://doi.org/10.1016/j.mineng.2021.107270.

References

Augustyn, A.R., Pott, R.W.M., Tadie, M., 2021. The interactions of the biosurfactant surfactin in coal flotation. Colloids Surf. A: Physicochem. Eng. Aspects 627, 127122. https://doi.org/10.1016/j.colsurfa.2021.127122.

Baccile, N., Seyrig, C., Poirier, A., Alonso-de Castro, S., Roelants, S.L.K.W., Abel, S., 2021. Self-assembly, interfacial properties, interactions with macromolecules and molecular modelling and simulation of microbial bio-based amphiphiles (biosurfactants). A tutorial review. Green Chem. 23 (11), 3842–3944.

Bicak, O., Ekmekci, Z., Bradshaw, D.J., Harris, P.J., 2007. Adsorption of guar gum and CMC on pyrite. Miner. Eng. 20, 996–1002.

Blesa, M.A., Weisz, A.D., Morando, P.J., Salfity, J.A., Magaz, G.E., Regazzoni, A.E., 2000. The interaction of metal oxide surfaces with complexing agents dissolved in water. Coord. Chem. Rev. 196, 31–63.

Dhar, P., Chernyshova, I.V., Thornhill, M., Roelants, S., Soetaert, W., Kota, H.R., 2019a. Floatability of chalcopyrite by glycolipid biosurfactants as compared to traditional thiol surfactants. Tenside Surfactants Detergents 56, 429–435.

Dhar, P., Havskjold, H., Thornhill, M., Roelants, S., Soetaert, W., Kota, H.R., Chernyshova, I., 2021. Toward green flotation: interaction of a sophorolipid biosurfactant with a copper sulfide. J. Colloid Interface Sci. 585, 386–399.

Dhar, P., Thornhill, M., Kota, H.R., 2019b. Comparison of single and mixed reagent systems for flotation of copper sulphides from Nussir ore. Miner. Eng. 142, 105930. https://doi.org/10.1016/j.mineng.2019.105930.

Dhar, P., Thornhill, M., Kota, H.R., 2019c. Investigation of copper recovery from a new copper deposit (Nussir) in Northern Norway. Miner. Process. Extr. Metall. Rev. 40 (6), 380–389.

Didyk, A.M., Sadowski, Z., 2012. Flotation of serpentinite and quartz using biosurfactants. Physicochem. Probl. Miner. Process. 48, 607–618.

Fainerman, V.B., Möbius, D., Miller, R., 2001. Surfactants: Chemistry, Interfacial Properties, Applications, 1first ed. Elsevier, New York, Amsterdam.

Fazaelipoor, M.H., Khoshdast, H., Ranjbar, M., 2010. Coal flotation using a biosurfactant from Pseudomonas aeruginosa as a frother. Korean J. Chem. Eng. 27 (5), 1527–1531. https://doi.org/10.1007/s11814-010-0223-6.

Fuerstenau, D.W., Urbina, R.H., 1987. Flotation fundamentals. In: Somasundaran, P., Moudgil, B.M. (Eds.), Reagents in Mineral Technology. Marcel Dekker Inc, New York, pp. 1–38.

Galet, L., Patry, S., Dodds, J., 2010. Determination of the wettability of powders by the Washburn capillary rise method with bed preparation by a centrifugal packing technique. J. Colloid Interface Sci. 346 (2), 470–475.

Gaudin, A.M., Fuerstenau, D.W., 1955. Quartz flotation with cationic collectors. Trans. Am. Inst. Min. Metall. Eng. 202, 958–962.

Hirata, Y., Ryu, M., Oda, Y., Igarashi, K., Nagatsuka, A., Furuta, T., Sugiura, M., 2009. Novel characteristics of sophorolipids, yeast glycolipid biosurfactants, as biodegradable low-foaming surfactants. J. Biosci. Bioeng. 108 (2), 142–146.

Hollenbach, R., Völp, A.R., Höfert, L., Rudat, J., Ochsenreither, K., Willenbacher, N., Syldatk, C., 2020. Interfacial and foaming properties of tailor-made glycolipids—influence of the hydrophilic head group and functional groups in the hydrophobic tail. Molecules 25 (17), 3797. https://doi.org/10.3390/molecules25173797.

Jain, G., Havskjold, H., Dhar, P., Ertesvåg, H., Chernyshova, I., Kota, H.R., 2020. Green Foam-Based Methods of Mineral and Ion Separation. In: Chernyshova, I., Ponnurangam, S., Liu, Q. (Eds.), Multidisciplinary Advances in Efficient Separation Processes. American Chemical Society, pp. 265–301.

Khoshdast, H., Sam, A., Vali, H., Noghabi, K.A., 2011. Effect of rhamnolipid biosurfactants on performance of coal and mineral flotation. Int. Biodeteriorat. Biodegrad. 65 (8), 1238–1243.

Khoshdast, H., Sam, A., Manafi, Z., 2012. The use of rhamnolipid biosurfactants as a frothing agent and a sample copper ore response. Miner. Eng. 26, 41–49.

Koh, A., Gross, R., 2016. Molecular editing of sophorolipids by esterification of lipid moieties: effects on interfacial properties at paraffin and synthetic crude oil-water interfaces. Colloids Surf. A: Physicochem. Eng. Asp. 507, 170–181.

Koh, A., Todd, K., Sherbourne, E., Gross, R.A., 2017. Fundamental characterization of the micellar self-assembly of sophorolipid esters. Langmuir 33 (23), 5760–5768.

Langevin, D., 2017. Aqueous foams and foam films stabilised by surfactants. Gravity-free studies. Comptes Rendus Mécanique 345 (1), 47–55.

Liu, Q., Zhang, Y.H., Laskowski, J.S., 2000. The adsorption of polysaccharides onto mineral surfaces: an acid/base interaction. Int. J. Miner. Process. 60, 229–245.

Lunkenheimer, K., Malysa, K., Winsel, K., Geggel, K., Siegel, S.t., 2010. Novel method and parameters for testing and characterization of foam stability. Langmuir 26 (6), 3883–3888.

Małysa, K., 1992. Wet foams: formation, properties and mechanism of stability. Adv. Colloid Interface Sci. 40, 37–83.

Moreira, G.F., Pecanha, E.R., Monte, M.B.M., Leal, L.S., Stavale, F., 2017. XPS study on the mechanism of starch-hematite surface chemical complexation. Miner. Eng. 110, 96–103.

Nagaraj, D.R., Farinato, R.S. and Arinaitwe, E., 2019. Flotation Chemicals and Chemistry. In: Dunne, R.C., Kawatra, K.S., Young, C.A. (Eds.), SME Mineral Processing and Extractive Metallurgy Handbook. Society for Mining, Metallurgy & Exploration, Englewood, Colorado, pp. 967–1010.

Olivera, C.A.C., Merma, A.G., Torem, M.L., 2019. Evaluation of hematite and quartz flotation kinetics using surfactant produced by Rhodococcus erythropolis as bioreagent [online] REM – Int. Eng. J. 72 (4), 655–659. https://doi.org/10.1590/0370-44672018720162.

Pearson, R.G., 1963. Hard and soft acids and bases. J. Am. Chem. Soc. 85, 3533–3539.

Penfold, J., Thomas, R.K., Shen, H.-H., 2012. Adsorption and self-assembly of biosurfactants studied by neutron reflectivity and small angle neutron scattering: glycolipids, lipopeptides and proteins. Soft Matter 8 (3), 578–591.

Pereira, A.R.M., Hacha, R.R., Torem, M.L., Merma, A.G., Silvas, F.P., 2021. Direct hematite flotation from an iron ore tailing using an innovative biosurfactant. Sep. Sci. Technol. 1–11.

Ponnurangam, S., Chernyshova, I.V., Somasundaran, P., 2012. Rational design of interfacial properties of ferric (hydr)oxide nanoparticles by adsorption of fatty acids from aqueous solutions. Langmuir 28 (29), 10661–10671.

Pugh, R., Stenius, P., 1985. Solution chemistry studies and flotation behaviour of apatite, calcite and fluorite minerals with sodium oleate collector. Int. J. Miner. Process. 15, 193–218.

Qiu, X.M., Yang, H.Y., Chen, G.B., Luo, W.J., 2019. An alternative depressant of chalcopyrite in Cu-Mo differential flotation and its interaction mechanism. Minerals 9 (1), 1. https://doi.org/10.3390/min9010001.

Rao, K.H., Vilinska, A., Chernyshova, I.V., 2010. Minerals bioprocessing: R & D needs in mineral biobeneficiation. Hydrometallurgy 104, 465–470.

Rath, R.K., Subramanian, S., Pradeep, T., 2000. Surface chemical studies on pyrite in the presence of polysaccharide-based flotation depressants. J. Colloid Interface Sci. 229 (1), 82–91.

Roelants, S.L.K.W., Ciesielska, K., De Maeseneire, S.L., Moens, H., Everaert, B., Verweire, S., Denon, Q., Vanlerberghe, B., Van Bogaert, I.N.A., Van der Meeren, P., Devreese, B., Soetaert, W., 2016. Towards the industrialization of new biosurfactants: Biotechnological opportunities for the lactone esterase gene from Starmerella bombicola. Biotechnol. Bioeng. 113 (3), 550–559.

Ross, V.E., 1989. Determination of the contributions by true flotation and entrainment during the flotation process. Int. Colloquium: Developments in Froth Flotation. Southern African Institute of Mining and Metallurgy, Gordon's Bay, South Africa.

Rosen, M., Kunjappu, J., 2012. Foaming and Antifoaming by Aqueous Solutions of Surfactants, Surfactants and Interfacial Phenomena, fourth ed. John Wiley & Sons Inc, Hoboken, pp. 308–335.

Schramm, L.L., Marangoni, D.G., 1994. Surfactants and their solutions: basic principles. In: Schramm, L.L. (Ed.), Foams: Fundamentals and Applications in the Petroleum Industry. American Chemical Society, Washington, DC, p. 13.

Somasundaran, P., Shrotri, S., Huang, L., 1998. Thermodynamics of adsorption of surfactants at solid-liquid interface. Pure Appl. Chem. 70, 621–626.

Szymanska, A., Sadowski, Z., 2010. Effects of biosurfactants on surface properties of hematite. Adsorption 16 (4-5), 233–239.

Theander, K., Pugh, R.J., 2001. The influence of pH and temperature on the equilibrium and dynamic surface tension of aqueous solutions of sodium oleate. J. Colloid Interface Sci. 239 (1), 209–216.

Valotteau, C., Calers, C., Casale, S., Berton, J., Stevens, C.V., Babonneau, F., Pradier, C.-M., Humblot, V., Baccile, N., 2015. Biocidal properties of a glycosylated surface: sophorolipids on Au(111). ACS Appl. Mater. Interfaces 7, 18086–18095.

Van Renterghem, L., Roelants, S.L.K.W., Baccile, N., Uytterspro, K., Taelman, M.C., Everaert, B., Mincke, S., Ledegen, S., Debrouwer, S., Scholtens, K., Stevens, C.,

Soetaert, W., 2018. From lab to market: an integrated bioprocess design approach for new-to-nature biosurfactants produced by Starmerella bombicola. Biotechnol. Bioeng. 115 (5), 1195–1206.
Warren, L.J., 1985. Determination of the contributions of true flotation and entrainment in batch flotation tests. Int. J. Min. Process. 14, 33–44.
Zouboulis, A.I., Matis, K.A., Lazaridis, N.K., Golyshin, P.N., 2003. The use of biosurfactants in flotation: application for the removal of metal ions. Miner. Eng. 16, 1231–1236.